Note: Fast imaging of DNA in atomic force microscopy enabled by a local raster scan algorithm

Peng Huang and Sean B. Andersson

Citation: Review of Scientific Instruments **85**, 066101 (2014); doi: 10.1063/1.4881682
View online: http://dx.doi.org/10.1063/1.4881682
View Table of Contents: http://scitation.aip.org/content/aip/journal/rsi/85/6?ver=pdfcov
Published by the AIP Publishing

Note: Fast imaging of DNA in atomic force microscopy enabled by a local raster scan algorithm

Peng Huang[1,a)] and Sean B. Andersson[2,b)]
[1]*Western Digital Technologies, Irvine, California 92612, USA*
[2]*Department of Mechanical Engineering and Division of Systems Engineering, Boston University, Boston, Massachusetts 02215, USA*

(Received 2 February 2014; accepted 23 May 2014; published online 5 June 2014)

Approaches to high-speed atomic force microscopy typically involve some combination of novel mechanical design to increase the physical bandwidth and advanced controllers to take maximum advantage of the physical capabilities. For certain classes of samples, however, imaging time can be reduced on standard instruments by reducing the amount of measurement that is performed to image the sample. One such technique is the local raster scan algorithm, developed for imaging of string-like samples. Here we provide experimental results on the use of this technique to image DNA samples, demonstrating the efficacy of the scheme and illustrating the order-of-magnitude improvement in imaging time that it provides. © *2014 AIP Publishing LLC*. [http://dx.doi.org/10.1063/1.4881682]

In the standard approach to imaging in atomic force microscopy (AFM), the tip of the instrument is raster-scanned across the sample and the image acquired pixel-by-pixel. The imaging rate is limited by a variety of factors[1,2] and most techniques for creating high-speed AFM (HS-AFM) rely on combinations of novel actuators and advanced controllers.[3,4] Efforts on actuators and mechanical design of the instrument push the physical speed that can be achieved both in lateral scanning and vertical motion of the cantilever[5,6] while novel controllers allow full use of that speed.[2,7] There has also been interest in developing novel scan patterns that fully cover the scan area faster than a standard raster pattern.[8,9]

These approaches to high-speed AFM scan in an open-loop fashion. The scan pattern is fixed and the focus is on moving the tip faster while maintaining image quality. It can be difficult or impossible to retrofit existing instruments with new hardware and the use of advanced controllers often requires specialized experience.

For samples sparsely distributed on the surface, the use of open-loop scan patterns implies that most of the imaging time is wasted measuring the substrate rather than the sample of interest. Motivated by this, we previously developed a local raster scan (LRS) algorithm for imaging string-like samples such as DNA, actin, microtubules, nanotubes, and the boundary of structures such as cells and crystals.[10] Here we present the first experimental results on λ-DNA, demonstrating an order-of-magnitude improvement in imaging rate on a standard AFM.

LRS uses the measurements in real time to estimate the spatial path of the sample being imaged. From the sample path prediction, $r(\cdot)$, the scan path is given by

$$r_{tip}(t) = r(s) \pm A \sin(\omega t) q_2(t), \tag{1}$$

where $q_2(t)$ describes a direction transverse to the sample (determined from the estimate), and A and ω are user-selected parameters that define the scan size and scan spatial resolution, respectively. This trajectory drives the tip to raster back and forth with an orientation that changes with the sample. A threshold detector based on a signal containing the edge information of the sample determines when the tip crosses the sample. At scan rates consistent with good height imaging, the amplitude signal can be used while at higher scan rates, signals derived from the cantilever motion are needed.[11] Each time the detector indicates an edge crossing, the predicted sample path is updated and filtered, thus closing the loop and making the algorithm robust to noise.

Since the tip is kept near the sample of interest, the time to acquire an image is reduced not by increasing the tip speed but by focusing the measurements where they are needed. Simulations and experiments on simulated and calibration samples in Refs. 10 and 12, as well as the experiments on DNA described below, demonstrate at least an order of magnitude improvement in scanning time without any physical alteration to the instrument. The primary trade-offs are that the algorithm relies on the sample having a string-like character and that data are gathered only local to the sample. One possible application, then, is high-speed repeated imaging of the same string to study dynamics on or of the sample. Due to the feedback nature of the scheme, effects such as creep and thermal drift are automatically compensated for.

Implementation of the LRS scheme, while not trivial, is straightforward. Access is needed to the signal used for threshold detection as well as to the drive of the scanning stage. Since the acquired data are not regularly spaced, interpolation is needed to generate an image from the measurements.[13]

Experiments were performed on an Agilent 5500 AFM equipped with a MAC III module and operated in its Acoustic AC mode. The cantilever used had a resonant frequency of 75 kHz and a spring constant of 2.8 N/m. The manufacturer's specifications give the bandwidth of the closed-loop

a)This research was performed while P. Huang was with the Department of Mechanical Engineering, Boston University, Boston, Massachusetts 02215, USA.
b)Electronic mail: sanderss@bu.edu.

in the z-direction to be around 1 kHz. To customize the scan trajectory, the Agilent controller for the x-y directions was disabled (through software). The open-loop systems in both x and y were measured in the frequency domain and a low level PI controller was developed. The resulting closed-loop system had a bandwidth of approximately 100 Hz. The z-direction was controlled with the standard Agilent software.

The data acquisition and the implementation of the algorithm and of the controller for the scanner were done using a compact Reconfigurable Input-Output (cRIO) system (cRIO 9082, National Instruments). This system includes an embedded 1.33 GHz real-time processor and an LX150 FPGA from the Xilinx Spartan-6 family as well as A/D converters (sampling rate up to 1 Ms/s) and a D/A converter (sampling rate of 100 ks/s). Edge detection was done using a threshold test on the amplitude signal; the threshold was selected through experience.

A sample of λ-DNA was diluted in purified water to a concentration of 50 μg/ml. A quantity of 30 μl was deposited on a freshly cleaved mica substrate, incubated for 5 min to allow the DNA to adhere to the substrate, and then flushed using 1 ml of purified water. The sample was then dried in air for 24 h.

Here we show two examples of LRS scanning on λ-DNA to illustrate the effectiveness and robustness of our algorithm. To show that the LRS approach can be used in any imaging mode, we present amplitude signal (rather than height) images; these also enhance the contrast in the DNA images. Note that one can generate topography and phase images as long as access to such signals are available. To initialize the scan (and to provide a reference for comparison), a standard raster scan of a 2.6 μm × 2.6 μm region with a 512 × 512 pixel resolution at a line rate of 2 lines/s was acquired and an initial position for the LRS scan indicated by clicking on the image. The average tip speed during the raster scan was 10.4 μm/s. To ensure the full width of the DNA was scanned, the amplitude parameter was set to $A = 50$ nm while the spatial period parameter was set to $\omega = (1/3)$ nm^{-1}. The tip speed was set to 10 μm/s to match approximately the tip speed during the raster scan.

Results from the first example are shown in Fig. 1. A portion of the full raster scan image is shown in Fig. 1(a) with a red circle indicating the desired initial position for the LRS image. The LRS took only 8 s, terminating when the tip encountered the large debris on the sample at approximately 1.2 μm in x and −0.7 μm in y. A standard raster scan of this same region would have taken approximately 120 s. The measured amplitude and edge detection signals are shown in Fig. 1(b); the zoom-in clearly shows the clean detection of the edges. The trajectory of the tip is shown in Fig. 1(d), though due to the high spatial resolution of the scan, it is difficult to make out details of the scan pattern. The image generated from the scan is shown in Fig. 1(c). Note that the scan crossed over two branch points during the scan. Due to a low pass filter in the LRS algorithm,[10] the straighter branch was followed each time.

Results from the second example are shown in Fig. 2. The initial position for the LRS scan is indicated by a red circle in Fig. 2(a). The scan was terminated after 7 s. A conventional raster scan of this same sample would have taken approximately 100 s. As shown in the inset in Fig 2(b), detection of the edge of the sample was lost during the scan due to loss of contrast in the amplitude signal arising in part from the noisy substrate. Because of the low pass filter in the algorithm,

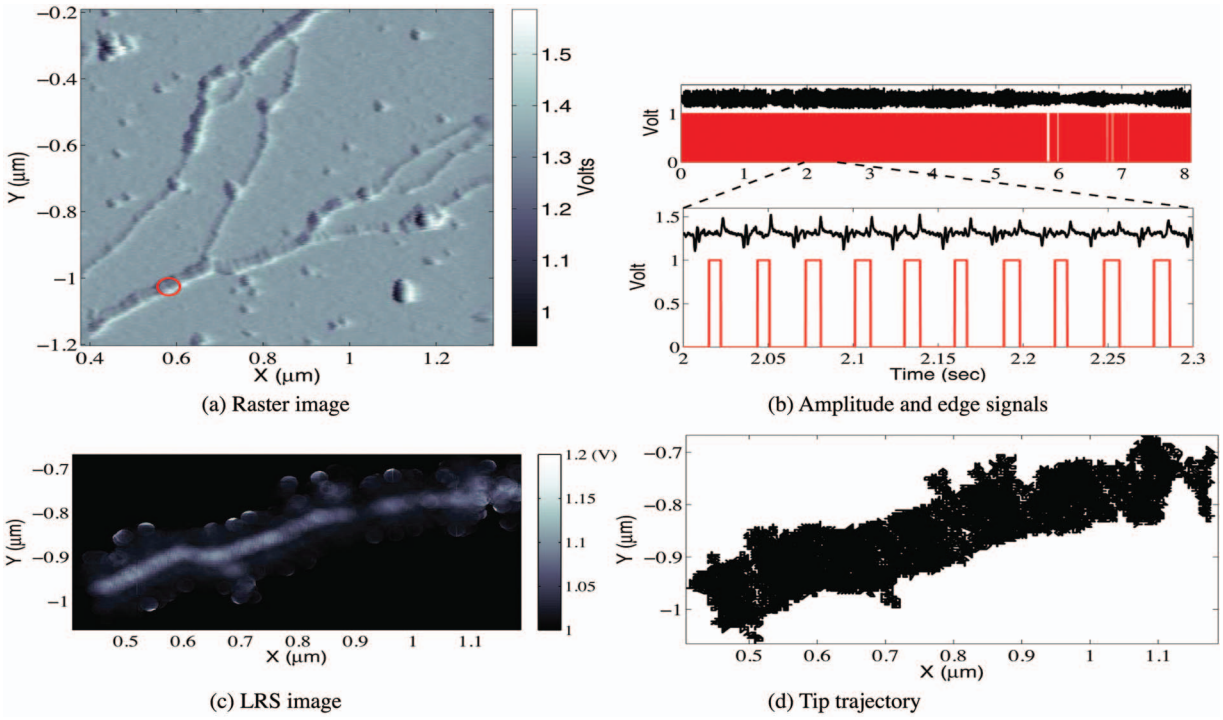

FIG. 1. Results on λ-DNA. (a) The original raster scan image. The circle (red) indicates the selected initial position for the LRS scan. (b) The amplitude (top, black) and edge detection (bottom, red) signals with a zoom-in to clearly show the signal features. (c) The LRS image generated from the scan. (d) The scan trajectory. Total LRS scan time was 8 s.

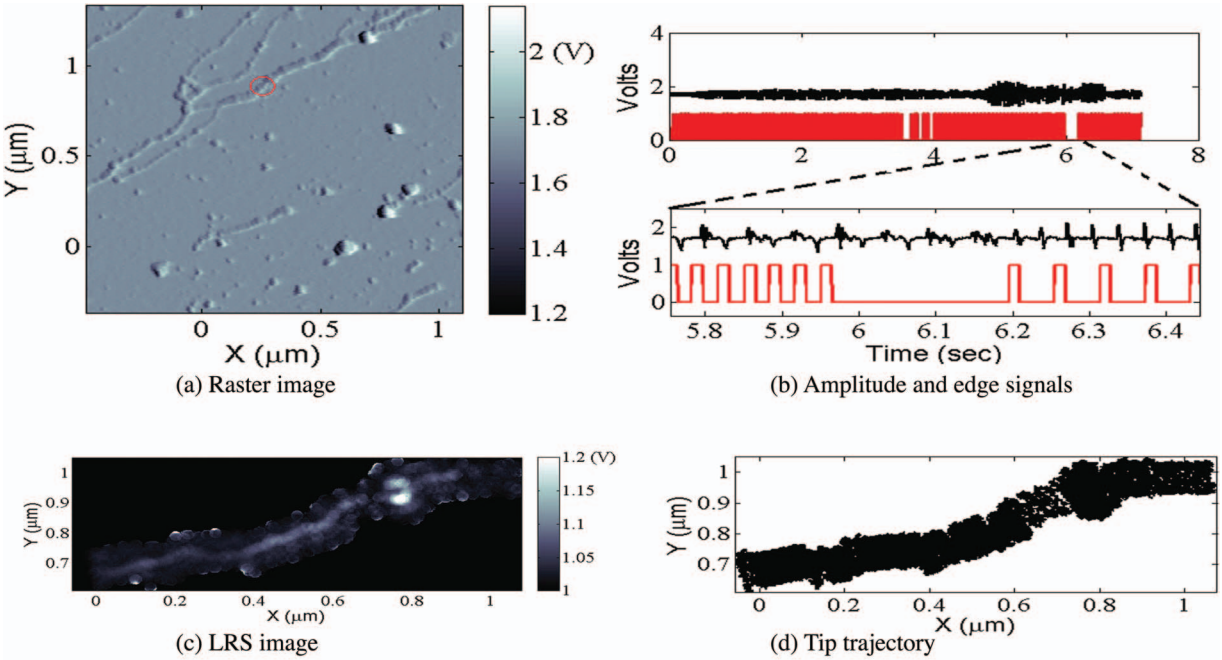

FIG. 2. Results on λ-DNA. (a) The original raster scan image. The circle (red) indicates the selected initial position for the LRS scan. (b) The amplitude (top, black) and edge detection (bottom, red) signals with a zoom-in to clearly show the signal features. (c) The LRS image generated from the scan. (d) The scan trajectory. Total LRS scan time was 7 s.

the tip continued along using the previous estimate until the detection signal appeared again. The feedback nature of the scheme then adjusted for any estimation errors accumulated during the period of missing detections such that the DNA was accurately imaged even after this event.

As seen in Figs. 1 and 2(a), the conventional raster scan gives a broader view of the sample of interest than the imaging result of the LRS in Figs. 1 and 2(c). Often, however, we are interested in dynamics occurring along one individual DNA string or other biopolymer, such as HS-AFM movies of myosin V moving on actin.[14] As indicated above, a standard raster scan covering the equivalent area of the DNA in Figs. 1(c) and 2(c) would take over ten times longer, illustrating the order-of-magnitude improvement achieved by taking advantage of the structure of the sample to be imaged. Further, these gains were achieved on a standard instrument and the technique is complementary to other HS-AFM schemes. The order-of-magnitude improvement is thus with respect to the standard imaging rate of the instrument being used.

The experimental results on DNA show that the LRS algorithm is robust to disturbances generated by debris on the sample surface and illustrates the feasibility of using LRS imaging. It can be applied to any existing instrument that provides access to the signals for detection and the command input to the scanner.

This work was supported in part by NSF through Grant No. CMMI-0845742 and by grants from the National Center for Research Resources (5R21RR025362-03) and the National Institute of General Medical Sciences (8 R21 GM103530-03) from the National Institutes of Health.

[1]Y. K. Yong, S. O. R. Moheimani, B. J. Kenton, and K. K. Leang, Rev. Sci. Instrum. **83**, 121101 (2012).
[2]T. Tuma, A. Sebastian, J. Lygeros, and A. Pantazi, IEEE Control Syst. Mag. **33**, 68 (2013).
[3]G. Schitter and M. J. Rost, Mater. Today **11**, 40 (2008).
[4]T. Ando, Nanotechnology **23**, 062001 (2012).
[5]B. J. Kenton, A. J. Fleming, and K. K. Leang, Rev. Sci. Instrum. **82**, 123703 (2011).
[6]B. J. Kenton and K. K. Leang, IEEE/ASME Trans. Mech. **17**, 356 (2012).
[7]S. M. Salapaka and M. V. Salapaka, IEEE Control Syst. Mag. **28**, 65 (2008).
[8]T. Tuma, J. Lygeros, V. Kartik, A. Sebastian, and A. Pantazi, Nanotechnology **23**, 185501 (2012).
[9]I. A. Mahmood, S. O. R. Moheimani, and B. Bhikkaji, IEEE Trans. Nanotech. **10**, 203 (2011).
[10]P. I. Chang, P. Huang, J. Maeng, and S. B. Andersson, Rev. Sci. Instrum. **82**, 063703 (2011).
[11]P. Huang and S. B. Andersson, in *Proceedings of IFAC Symposium on Mechatronics* (IFAC, 2013), pp. 153–160.
[12]P. Huang and S. B. Andersson, in *Proceedings of American Control Conference* (IEEE, 2013), pp. 6063–6068.
[13]P. Huang and S. B. Andersson, in *Proceedings of American Control Conference* (IEEE, 2011), pp. 2246–2251.
[14]N. Kodera, D. Yamamoto, R. Ishikawa, and T. Ando, Nature (London) **468**, 72 (2010).